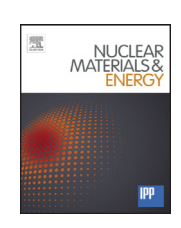
Nuclear Materials and Energy 000 (2016) 1-5



Contents lists available at ScienceDirect

## Nuclear Materials and Energy

journal homepage: www.elsevier.com/locate/nme



## Microstructural defects in EUROFER 97 after different neutron irradiation conditions

Christian Dethloff\*, Ermile Gaganidze, Jarir Aktaa

Karlsruhe Institute of Technology (KIT), Institute for Applied Materials (IAM), Hermann-von-Helmholtz-Platz 1, 76344 Eggenstein-Leopoldshafen, Germany

#### ARTICLE INFO

Article history: Received 13 November 2015 Revised 11 April 2016 Accepted 17 May 2016 Available online xxx

Keywords:

Transmission electron microscopy (TEM) RAFM steels Irradiation defects Microstructural analysis

#### ABSTRACT

Characterization of irradiation induced microstructural evolution is essential for assessing the applicability of structural steels like the Reduced Activation Ferritic/Martensitic steel EUROFER 97 in upcoming fusion reactors. In this work Transmission Electron Microscopy (TEM) is used to determine the defect microstructure after different neutron irradiation conditions. In particular dislocation loops, voids and precipitates are analyzed concerning defect nature, density and size distribution after irradiation to 15 dpa at 300 °C in the mixed spectrum High Flux Reactor (HFR). New results are combined with previously obtained data from irradiation in the fast spectrum BOR-60 reactor (15 and 32 dpa, 330 °C), which allows for assessment of dose and dose rate effects on the aforementioned irradiation induced defects and microstructural characteristics.

> © 2016 Published by Elsevier Ltd. This is an open access article under the CC BY-NC-ND license (http://creativecommons.org/licenses/by-nc-nd/4.0/).

#### 1. Introduction

Neutron irradiation deteriorates mechanical properties of structural materials by both modifying the existing microstructure and inducing new microstructural defect types. Even though reduced activation ferritic/martensitic (RAFM) steels like the European variant EUROFER 97 are especially designed for withstanding the harsh environment in future fusion reactors, they still suffer from low temperature hardening and embrittlement which limit their application. Therefore characterization of microstructural evolution and induced defects under irradiation is the key for understanding irradiation effects and correlating subsequent changes in mechanical properties.

Since irradiation in a fusion like neutron spectrum is not available at present, different fission reactor irradiation experiments had been performed. Among these neutron irradiations, the SPICE experiment (300 °C, 15 dpa) [1,2] carried out in the mixed spectrum High Flux Reactor (HFR) of NRG in Petten, and the WTZ 01/577 (330 °C, 15 dpa) [3] and ARBOR1 experiment (330 °C, 32 dpa) [4] carried out in the BOR-60 fast reactor of SSC RIAR in Dimitrovgrad are of great importance for this work (for detailed specifications of irradiation experiments see next section).

E-mail address: christian.dethloff@kit.edu (C. Dethloff). URL: http://www.iam.kit.edu/wbm (C. Dethloff)

http://dx.doi.org/10.1016/j.nme.2016.05.009

\* Corresponding author.

EUROFER 97 in the unirradiated reference state has been characterized concerning material and mechanical properties [5,6] and microstructural stability under thermal annealing [7]. Irradiation influence on microstructure was determined concerning dislocation loops and voids after WTZ 01/577 and ARBOR1 [8] and after SPICE [9], and precipitates [10] after ARBOR1 irradiation. Analyses on helium bubbles were performed on boron doped [11] EUROFER 97 based steels, where boron artificially increased helium generation to a value comparable to fusion conditions, after ARBOR1 [12] and SPICE [13] irradiation. The correlation of irradiation defects with change in mechanical properties of EUROFER 97 has been recently assessed [14] making use of appropriate hardening models like the Dispersed Barrier Hardening (DBH) model [15].

In this work, new results on irradiation defects microstructure are presented. The investigation completes characterizations of different defect types concerning sizes and densities for the different irradiation experiments and addresses existing disagreement in previous publications.

#### 2. Experimental procedure and technique

The basic material used in this work is the RAFM steel EU-ROFER 97 (rolled plate material, heat 83697) produced by Böhler Austria GmbH with a composition of 8.91 Cr 1.08 W 0.48 Mn 0.20 V 0.14 Ta 0.006 Ti 0.12 C (wt.%, Fe balance) [16]. The material was delivered in a normalized (980 °C for 0.5 h) and tempered (760 °C for 1.5 h) condition. Several types of mechanical testing

2352-1791/© 2016 Published by Elsevier Ltd. This is an open access article under the CC BY-NC-ND license (http://creativecommons.org/licenses/by-nc-nd/4.0/).

**Table 1** Specifications of irradiation experiments. Detailed information can be found in [1-4].

Experiment	SPICE	WTZ 01/577	ARBOR1
Irradiation facility Dose (dpa) Neutron flux (E>0.1 MeV) (m <sup>-2</sup> s <sup>-1</sup> )	HFR Petten 15 4.0 × 10 <sup>18</sup>	BOR-60 15 1.8 × 10 <sup>19</sup>	BOR-60 32 1.8 × 10 <sup>19</sup>
Neutron flux (Thermal) (m <sup>-2</sup> s <sup>-1</sup> )	$1.4\times10^{18}$	-	-
Irradiation temp. (°C)	300	330	330

specimens were neutron irradiated in the irradiation experiments SPICE, WTZ 01/577 and ARBOR1: the corresponding irradiation specifications are shown in Table 1.

TEM samples were manufactured in the Hot Cells at the Fusion Materials Laboratory (FML) of KIT from undeformed parts of irradiated EUROFER 97 impact test specimens with a cross-sectional area of 3  $\times$  4 mm². By using a cutting wheel slices with thicknesses of about 150–200 $\mu$  m were prepared and subjected to electrolytic polishing in a solution of 20%  $\rm H_2SO_4$  + 80% CH\_3OH at room temperature with a Tenupol-5 jet polisher. Afterwards, in order to minimize radioactivity and also the influence of the magnetic sample on the electron beam, discs of only 1 mm in diameter including the electron-transparent region were punched out. A foldable copper net carried the 1 mm sample and was used for examination in the TEM.

TEM investigations were performed at 200 kV on a high resolution FEI Tecnai G<sup>2</sup> F20 X-TWIN microscope equipped with a postcolumn GIF Tridiem energy filter and located in the Hot Cells at FML. Prior to each investigation the surface contamination of the TEM specimens was reduced by applying a plasma cleaning treatment of 10 min with air plasma. In TEM mode, all images were recorded with the GIF camera and zero-loss filtered with an energy slit of 15 eV to improve contrast. In scanning TEM (STEM), nanoprobe mode was used resulting in a probe diameter of approximately 1.5 nm, and images were processed by a High Angle Annular Dark-Field (HAADF) detector. Elemental analysis by Energy Dispersive X-ray spectroscopy (EDS) was performed. For defect density evaluation the foil thickness of the investigated regions was determined by Convergent Beam Electron Diffraction (CBED) [17,18], and the recorded CBED patterns were analyzed using a DigitalMicrograph<sup>TM</sup> script [19].

#### 3. Results

#### 3.1. Dislocation loops

The weak-beam dark-field (WBDF) technique [20] is used for imaging dislocation loops. The diffraction conditions, as given in Table 2, were chosen in such a way that an excitation error  $s_g$  of approximately  $0.2~\rm nm^{-1}$  was achieved. This allows for imaging of small defects down to 1 nm of size, since the diffraction contrast can be minimized and approaches to the real physical size of the dislocation loops. Fig. 1 shows a WBDF image of area 2 of SPICE specimen SPI-1 with diffraction conditions given in the figure caption. In the image enlargement some dislocation loops are marked by circles. Due to the invisibility criterion  $g \cdot b = 0$  only a fraction of dislocation loops are visible. Therefore different diffraction conditions are analyzed as shown in Table 2, the table also gives the invisible loop types for each condition.

Dislocation loop size distributions with a histogram bin size of 1 nm for all three diffraction conditions are presented in Fig. 2. Analyses for  $g = \{3 - 10\}$  and  $\{200\}$  show comparable dislocation loop size distributions. A peak around 3 nm is observed, with a

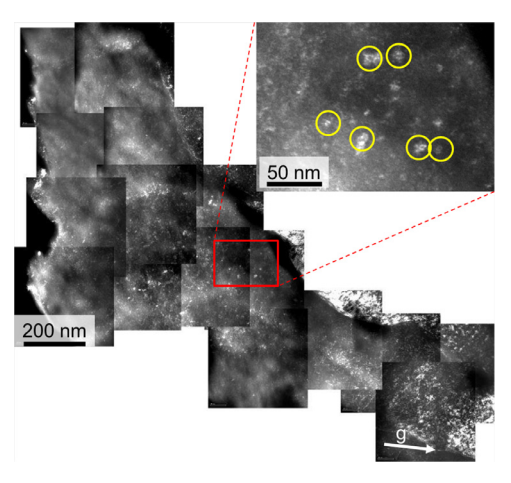


**Fig. 1.** TEM-WBDF micrograph showing investigated area 2 of sample SPI-1 after 15 dpa at 300°C. The WBDF images are taken near a [011] zone axis with g(3.1g),  $g = \{2 - 11\}$ . The red marked area is shown enlarged to visualize dislocation loops.

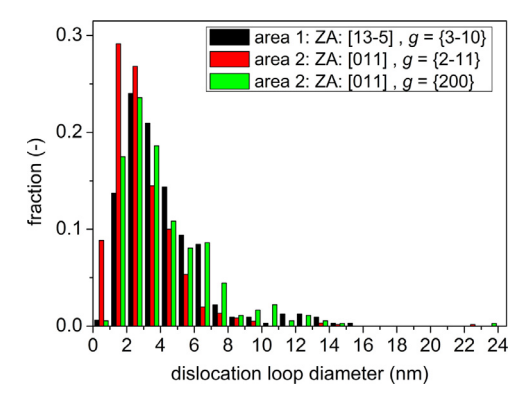


**Fig. 2.** Dislocation loop size distributions of sample SPI-1 after 15 dpa at 300°C for different diffraction conditions (see also Table 2).

small amount of larger loops exceeding 8 nm. The analysis for  $g=\{2-11\}$  differs however, since a much higher fraction of smallest loops below 2 nm is observed. Corresponding densities and mean diameters of visible dislocation loops are given in Table 2. Although identification and measurement of smallest loops is more difficult due to limited TEM resolution, results indicate that in general loops of type  $\frac{1}{2}\langle111\rangle$  are larger in size and less numerous than loops of type  $\langle100\rangle$  when taking into account the respectively visible loop types. The actual loop densities, despite the partial invisibility, can be estimated by solving a set of linear equations as proposed in [21]. Results give a dislocation loop density of  $N_{\langle100\rangle}=4.9\times10^{21}~\text{m}^{-3}$  and  $N_{\frac{1}{2}\langle111\rangle}=1.4\times10^{21}~\text{m}^{-3}$ , i.e. in total  $N_{\text{tot}}=6.3\times10^{21}~\text{m}^{-3}$ .

#### 3.2. Voids

Voids are identified and made visible by performing TEM bright-field (BF) through-focal series. From under- to overfocus, the diffraction contrast of voids changes from bright interior to dark, while the fresnel fringes change contrast vice versa [22]. Fig. 3 shows the void size distribution after 15 dpa at 300°C in SPICE specimen SPI-1. In the overlay voids can be observed in underfocus condition with a focus of  $-1\mu$  m. Voids are homogeneously distributed in the matrix after irradiation, no preferential nucleation sites are observed. Mean void diameter is 2.3 nm, the void density is determined as  $6.3 \times 10^{21}$  m<sup>-3</sup>.

### Download English Version:

# https://daneshyari.com/en/article/7987661

Download Persian Version:

https://daneshyari.com/article/7987661

<u>Daneshyari.com</u>